

# Binarization of a super-resolving graytone pupil filter by digital halftoning

Marek Kowalczyk  
Tomasz Cichocki  
Manuel Martínez-Corral

**Abstract** — Six digital-halftoning procedures, including one algorithm proposed by us, are compared to determine which one is best suited to binarization of a parabolic super-resolving pupil filter. The procedures we deal with include iterative, error-diffusion, error-convergence, and 1-pixel algorithms. We carry out a numerically simulated experiment in which an object that consists of either one point source or two coherent point sources is imaged in a  $4f$  imaging system with either a continuous super-resolving parabolic filter or one of its six different binary versions. The performance of binary filters is examined in terms of two parameters: the resemblance of their amplitude impulse response (AIR) to the AIR of the original continuous filter, as well as the two-point Sparrow resolution criterion. We found that the best performance in terms of both figures of merit is achieved with the filter generated by means of one-weight error diffusion when the weight is randomly positioned and the algorithm is processed on a serpentine raster.

**Keywords** — Coherent imaging, digital halftoning, error diffusion, super-resolution.

## 1 Introduction

The performance of a linear coherent imaging system can be described either by means of its amplitude impulse response (AIR) or by the Fourier transform of this magnitude, *i.e.*, the coherent transfer function (CTF). In an optical experiment, we can directly shape the CTF by placing a filter in the pupil plane of the system, and in this way we can control the AIR. The design of pupil-plane filters (*e.g.*, apodizing filters, super-resolving filters, deblurring filters, etc.) was extensively studied in the past.<sup>1,2</sup> Nonetheless, the manufacture of continuous-tone pupil filters has remained a difficult task. An attractive solution of this problem is to fabricate pupil filters in binary form by means of high-resolution computer-controlled light plotters. Pupil filters binarized by some halftoning methods were successfully applied in line-scan image generators to shape read-and-write beams<sup>3</sup> and in confocal microscopy to provide high spatial resolution.<sup>4</sup> Therefore, the influence of the binarization procedure on the performance of a binary filter should be examined.

When binarization methods are used for creation of the illusion of continuous-tone pictures (halftoning), the resulting binary image is usually examined both in the spatial domain and in the Fourier domain. In the spatial domain, subjective visual criteria are applied. In the Fourier domain, isotropy, regularity, and extension of the spectrum of a uniformly gray object rendered with a given halftoning method are examined.<sup>5</sup> On the contrary, when binarization methods are used to implement the binary version of a pupil filter, the performance of the binary mask is evaluated only in the spatial frequency domain, where the Fourier spectrum of its

amplitude transmittance, *i.e.*, its AIR, is compared with the Fourier spectrum of the original continuous-tone filter.

A general analytic approach that enables us to predict how a binarization procedure affects the spectrum of a gray-tone filter is available for only three classes of halftone procedures. The first class consists of all the techniques based on the periodic carrier concept.<sup>3, 6-8</sup> The use of these methods for binarization of filters would strongly affect the resemblance between AIRs of binarized and continuous-tone pupil filters. This is because irrespective of the nature of the continuous-tone filter spectrum, the spectrum of the corresponding binary filter is periodic. Thus, those techniques will not be addressed here.

The second class consists of generalized deterministic (without stochastic perturbations<sup>5</sup>) error-diffusion (ED) procedures. A comprehensive analysis of the spectra of binarized images and diffractive optical elements obtained by means of these algorithms was presented in terms of filter theory by Weissbach and Wyrowski.<sup>9</sup>

The third class consists of procedures based on the random-carrier concept. A technique which belongs to this class is, for example, that presented by Mitsa and Parker<sup>10</sup> in which the halftoning is achieved by a pixelwise comparison of the gray-scale image to a blue-noise mask. In a recent work, we have presented a rigorous analytic description of dithering with a white-noise mask.<sup>11</sup> We showed that the statistical average of the AIR of a pupil filter binarized with this method is approximately equal to the AIR of the corresponding continuous-tone filter, provided that the number of transparent cells within the pupil is sufficiently large. Dithering with white noise has been the unique digital-

Received 12/17/94; accepted 3/21/95.

M. Kowalczyk is currently with the Department of Optics, University of Valencia, 46100 Burjassot, Spain. Permanent address: Image Processing Group, Institute of Geophysics, University of Warsaw, Pasteura 7, 02093, Warsaw, Poland; telephone 48-22-235281, fax 48-22-222387, e-mail: mkowalcz@plearn.edu.pl.

T. Cichocki is with the Image Processing Group, Institute of Geophysics, University of Warsaw, Warsaw, Poland.

M. Martínez-Corral is with the Department of Optics, University of Valencia, Burjassot, Spain.

© Copyright 1995 Society for Information Display 1071-0922/95/0302-0067\$1.00

halftoning method successfully applied to binarization of the amplitude transmittance of pupil filters.<sup>4</sup>

The aim of this paper was to find the binarization method which would yield, as closely as possible, similar spectra for a continuous-tone parabolic super-resolving pupil filter and its corresponding binary version. Since approximately 80% of the AIR energy is concentrated in its central maximum and low-order side lobes, we are looking for a procedure which would not affect the low-frequency part of the spectrum of the filter transmittance. There exist binarization methods whose actual implementation is well-adapted to our needs. This favorable situation results from the fact that in order to meet subjective criteria of human understanding of images, many halftone procedures have been optimized to give an isotropic blue-noise shape to the spectrum of binarization noise. The blue-noise spectrum of binarization noise means that the low-frequency part of the spectrum of a continuous-tone element remains practically unaffected when the binarization procedure is executed, which, by coincidence, is exactly our aim. The blue-noise shape of the spectrum is an inherent feature of all the ED procedures. It can also be achieved in some iterative halftone procedures in which the shape of a fixed part of the spectrum is directly controlled.

Since an analytical description of the influence of digital halftoning on the Fourier spectrum is available only for deterministic ED and for dithering with random carriers, we perform here a numerical experiment to compare the performance of the six binary versions of a super-resolving parabolic pupil-plane filter generated with six representative halftoning algorithms. A similar comparison study was done by Billotet-Hoffmann and Bryngdahl with respect to sine-wave pupils but only qualitative results were given.<sup>12</sup> We examine all the binary filters for the resemblance of their spectra to that of the continuous-tone filter and for the two-point resolution evaluated in terms of the Sparrow criterion.

In this way we, in fact, evaluate different halftoning techniques to choose one which best suits our needs. We use the Sparrow resolution criterion as a merit function for the following reasons. Any fabrication method can be evaluated directly and indirectly. By direct evaluation we mean the measurement of important parameters of the fabricated object – in the present case, the Fourier spectrum of the digitally halftoned pupil filter. By indirect evaluation, we mean the evaluation of the result that is achieved by using the object – here, the super-resolution that can be achieved with subsequent binary filters. In our opinion, a complete investigation should include both kinds of evaluation, if possible. There are areas, *e.g.*, pharmacy, where such an approach is quite common. There the therapeutic result is even more important than the physical and chemical properties of a medication.

The results of direct and indirect evaluation should, in principle, coincide or at least be highly correlated. The coincidence confirms that our understanding of a physical

situation is right and that we use an adequate mathematical model to describe it.

The lack of correlation stimulates further investigation to get better insight into the phenomena involved. We shall see that for a low degree of resemblance between corresponding spectra, there is no evident correlation between both of the merit functions we used. A possible explanation of this will be given in Section 4.

---

## 1.1 Some definitions

### 1.1.1 Pupil filter

A pupil filter is an absorbing or phase-shifting transparency placed on the pupil, usually the exit pupil, of an imaging system to properly shape the pupil function of the system. In the special case of the  $4f$  imaging system of Fig. 7, the filter is placed in the Fourier plane (the  $\mu, \nu$  plane), which does not coincide with either the entrance or exit pupil; these are at minus and plus infinity, respectively. Pupil filters are spatial-frequency filters. They are neither color nor holographic filters. Color filters or holographic filters sometimes occupy pupil-filter positions (pseudocoloring, pattern recognition), but in such cases they are not referred to as pupil filters. Sometimes pupil filters occupy extrapupilar positions.<sup>13</sup>

---

### 1.1.2 The Sparrow criterion

Due to diffraction, the image of a point source produced by any real imaging system is not a bright point; it has a finite, non-zero size. The amplitude distribution within such a diffraction spot (*i.e.*, the amplitude impulse response of a system, also referred to as the *point-spread function*) is Fourier-conjugated with the pupil function of the system. The *pupil function* characterizes the system in the spatial-frequency domain and is equal to the properly normalized amplitude distribution, which appears just behind the exit pupil when the object to be imaged is a point source. By placing a transparency in the exit-pupil plane, *i.e.*, a pupil filter, we can modify the pupil function and therefore influence the point-spread function.

The question arises: what is the minimum separation  $2b$  (see Fig. 7) between two coherent point sources such that two overlapping point-spread functions could still be recognized as the image of a two-point object. The answer depends on the criterion we apply. According to the Sparrow resolution criterion, the lower limit of  $2b$  is that for which the second derivative of the resulting intensity distribution vanishes at the midpoint between geometrical (Gaussian) images of both sources. For an aberration-free correctly focused system with a clear (no filter) circular pupil,  $2b = 4.600$  in dimensionless normalized units.<sup>14</sup>

---

### 1.1.3 Super-resolution

If we properly attenuate the low-frequency transmission of the imaging system by means of a pupil filter (such manipu-

lations performed in the pupil are known as *apodization*), we can overcome the above limit to obtain  $2b < 4.600$ . This is referred to as super-resolution in the sense of the Sparrow criterion.

### 1.1.4 Parabolic super-resolving filter

A parabolic super-resolving filter is a rotationally symmetric pupil filter whose amplitude transmission is a parabolic function of the radial coordinate [Eq. (S)]. Such a filter eliminates the zero frequency and considerably attenuates low frequencies. The frequencies closest to the cutoff frequency remain virtually unaffected.

### 1.1.5 Blue noise

Blue noise (terminology introduced in Ref. 5) is high-frequency white noise devoid of low-frequency energy.

## 2 Description of the algorithms

A large number of two-dimensional digital-half-toning techniques which are good blue-noise generators have been reported in the literature.<sup>5</sup> Here we limit our interest to five of them representing different approaches. We also test the dithering with white noise, which, as the unique digital-half-toning procedure recommended until now for binarization of pupil filters, can be considered a reference point. In this way, we study the performance of the following binarization methods:

- (a) Dithering with white noise.<sup>11</sup>
- (b) ED with one weight which is randomly positioned.<sup>5</sup>
- (c) ED with Floyd and Steinberg error filter perturbed by an uniformly distributed bipolar additive white noise.<sup>5</sup>
- (d) ED with the Floyd and Steinberg filter perturbed by a properly scaled output of a symmetrical hard-clipper, with the noise generated in (c) used as the input.
- (e) Multiresolution error-convergence algorithm (MECA) with random choice of testing pixels.<sup>15</sup>
- (f) Iterative Fourier-transform algorithm (IFTA).<sup>16,17</sup>

Algorithm (a) is completely described in the literature, whereas algorithms (b), (c), (e), and (f) contain some free parameters that should be specified. Finally, algorithm (d) proposed here is a modification of (c). It was supposed to improve the performance of its original version.

For versions (b), (c), and (d), of the ED method, the algorithms are processed pixel by pixel on a serpentine raster (see Fig. 1).

In the case of ED with one randomly positioned weight [algorithm (b)], we select the position of the weight with equal probability between two candidate locations, immediately below and preceding the filter origin (Fig. 2).

In the case of ED with Floyd and Steinberg filter perturbed by white noise [algorithm (c)], we start with pairing

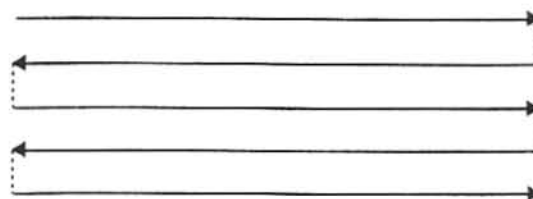


FIGURE 1 — Serpentine raster path.

original Floyd and Steinberg weights of comparable value. We form two pairs  $(1/16, 3/16)$  and  $(5/16, 7/16)$ . Then for each pixel two statistically independent random variables  $\chi$  and  $\psi$  are generated. The random variable  $\chi$  perturbs the  $(1/16, 3/16)$  pair and  $\psi$  perturbs the other pair. These random variables have the following uniform probability density functions:

$$p_{\chi}(\chi) = \begin{cases} 8 & -\frac{1}{16} \leq \chi \leq \frac{1}{16} \\ 0 & \text{otherwise} \end{cases} \quad (1)$$

and

$$p_{\psi}(\psi) = \begin{cases} 16 & -\frac{5}{16} \leq \psi \leq \frac{5}{16} \\ 0 & \text{otherwise.} \end{cases} \quad (2)$$

Next, we multiply  $\chi$  and  $\psi$  by  $b$  and  $b'$ , respectively, where  $b$  and  $b'$  belong to the  $[0,1]$  interval. Then  $b\chi$  and  $b'\psi$  perturb the corresponding pairs:

$$\left(\frac{1}{16}, \frac{3}{16}\right) \rightarrow \left(\frac{1}{16} + b\chi, \frac{3}{16} - b\chi\right) \quad (3)$$

and

$$\left(\frac{5}{16}, \frac{7}{16}\right) \rightarrow \left(\frac{5}{16} + b'\psi, \frac{7}{16} - b'\psi\right). \quad (4)$$

The scaling factors  $b$  and  $b'$  express the maximum percentage of the smaller weight in the pair affected by noise. In our experiment,  $b = b' = 0.5$ . Thus, in every sampled point of the pupil, we use the error filter shown in Fig. 3.

In our modification of the above binarization algorithm [*i.e.*, in algorithm (d)], the random variable  $\chi$  takes on

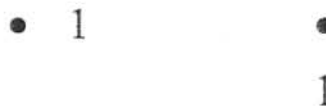


FIGURE 2 — Two one-weight error filters used when the row of pixels is processed from left to right. We select, with equal probability, one of them to diffuse the error from the origin position represented by a solid circle.

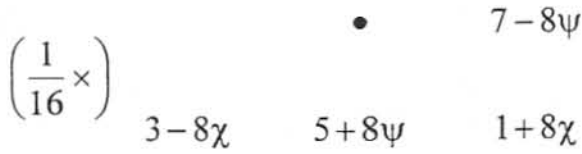


FIGURE 3 — Error filter used when the classical weights of Floyd and Steinberg are perturbed by a uniformly distributed bipolar additive white noise.

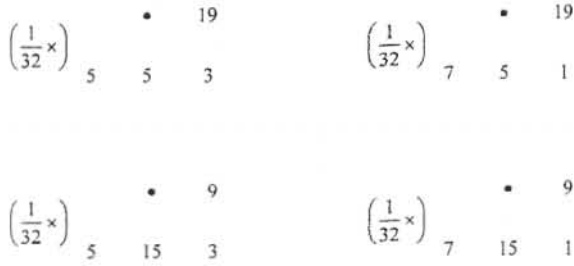


FIGURE 4 — Error filters used in the algorithm (d) for rows of pixels processed from left to right.

with equal probability only two values,  $-1/16$  and  $1/16$ , whereas the variable  $\psi$  takes on the values  $-5/16$  and  $5/16$ . Again we assume that  $\chi$  and  $\psi$  are statistically independent, so that in every point of the pupil filter we use with equal probability one of the four error filters presented in Fig. 4.

The MECA, algorithm (e), can be considered a symmetrical ED algorithm processed in parallel. Thus, it is sup-

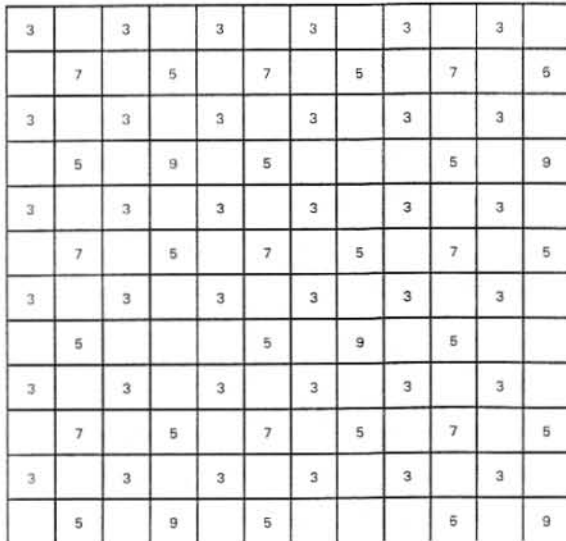


FIGURE 5 — Pixel positions tested for possible change of the binary assignment. Pixels are marked with odd numbers  $2n - 1$ , where  $n$  is the pyramid level and  $(2n - 1) \times (2n - 1)$  is the size of the window used for calculation of the weighted average error. The shaded area corresponds to a quadrant of the clear pupil used in our simulation. When algorithm (e) was executed, some of these pixel positions were randomly shifted according to the probability distribution given by Eq. (5).

TABLE 1 — Error thresholds used in the algorithm (e) to determine whether a pixel binary assignment should be changed.

Pyramid level			
2	3	4	5
64/255	36/255	10/255	3/255

posed to be free from directional hysteresis, which is typical for all ED methods processed sequentially. A distinctive feature of this algorithm is its pyramidal structure. At the first pyramid level, the original continuous-tone image is hard-clipped pixel by pixel to produce the binary image. At higher levels, the binarized image is compared with the continuous-tone image over a window of pixels for calculation of a weighted averaged error. Then, the binary assignment is changed if the weighted averaged error exceeds a threshold value that can be determined analytically or adjusted experimentally. In the comparison, we center the window at the selected binarized pixels (see Fig. 5). The theoretical and experimental threshold values do not coincide, and they both depend on the pyramid level. The number and distribution of tested pixels and the size of the window depend on the pyramid level. In our calculation we use five pyramid levels, and at each level we test a subset of pixels and apply the windows proposed by Peli for the basic version of MECA modified by pseudorandom perturbations [algorithm (e)].<sup>16</sup> The threshold values that we use are presented in Table 1.

The basic version of the multiresolution error-convergence algorithm has the drawback that when it renders some gray levels it yields false contours and directional patterns (textures). To reduce these effects, we follow Peli's idea of including pseudorandom noise in the choice of pixels to be tested at each pyramid level. In this case, the probability of shifting a tested point from its central position to any of eight neighboring positions is given by the matrix

$$M = \begin{bmatrix} 1/60 & 2/15 & 1/60 \\ 1/15 & 8/15 & 1/15 \\ 1/60 & 2/15 & 1/60 \end{bmatrix}. \quad (5)$$

From Eq. (5) almost 50% of the points to be tested are randomly shifted from the positions they occupy in the deterministic version of the algorithm.

In the IFTA [algorithm (f)], the binary transmittance is approached stepwise. We start with the continuous-tone transmittance  $t(u, v)$  and execute the iterative procedure according to the flow chart presented in Fig. 6. The operators  $\mathcal{U}$  and  $\mathcal{H}$  represent the constraints imposed on  $t_j(u, v)$  and on the Fourier transform of  $\mathcal{U}t_j(u, v)$ , which we denote  $T_j(x, y)$ . The operators are defined as follows:

$$\mathcal{U}^{(p)} t_j(u, v) = \begin{cases} 0, & |t_j(u, v)| \leq e^{(p)} & j = 0, 1, 2, \dots, 59 \\ 1, & |t_j(u, v)| > 1 - e^{(p)} & p = 1, 2, \dots, 46 \\ |t_j(u, v)|, & \text{otherwise} \end{cases} \quad (6)$$

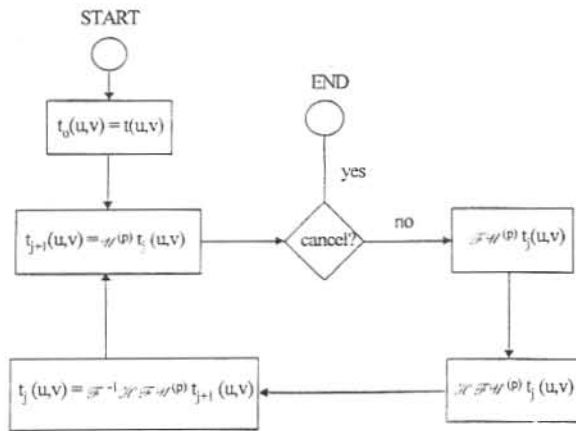


FIGURE 6 — Flow chart for the iterative Fourier-transform algorithm used to calculate binary filters.

and

$$\Re T_j(x,y) = \begin{cases} \beta_j |T(x,y)| \exp[i \arg\{T_j(x,y)\}], & (x,y) \in S \\ T_j(x,y), & \text{otherwise,} \end{cases} \quad (7)$$

where  $T(x,y)$  is the Fourier transform of  $t(x,y)$  and  $\beta_j$  is the proportionality constant that minimizes the quadratic deviation of  $T_j$  from  $T$  over the window  $S$ .<sup>17</sup> The area  $S$ , in which  $T_j(x,y)$  is substituted by  $\beta_j |T(x,y)| \exp[i \arg\{T_j(x,y)\}]$ , is bounded by the second zero ring in  $T(x,y)$ . The parameter  $e^{(p)}$  increases by 0.01 every 10 iterations within the range [0.05, 0.50]. In order to evaluate the direct and inverse Fourier transforms, we use the fast Fourier transform (FFT). For this purpose, binary filters, with diameters of 23 pixels each, are placed in the  $128 \times 128$  matrix of pixels.

Summarizing, procedure (a) has been chosen as a reference point because, of all the procedures applied to binarization of pupil functions, it has given the best results until now. Algorithms (b)–(d) have nearly blue-noise char-

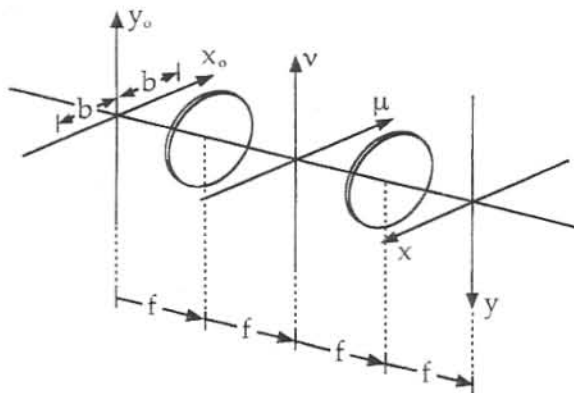


FIGURE 7 — The configuration assumed in our numerical experiment.

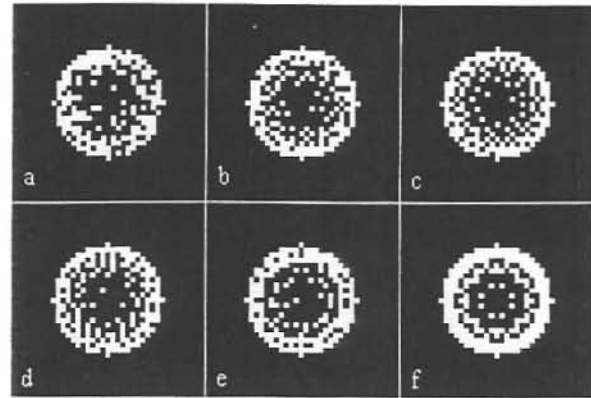


FIGURE 8 — Binary filters obtained with (a)–(f) algorithms.

acteristics. Algorithm (e) has a slightly poorer blue-noise spectrum and is more sensitive to edge effects, but on the other hand it is free from directional hysteresis. Finally, algorithm (f) has been chosen because it was designed to obtain a high degree of resemblance between the spectrum of a continuous-tone element and that of its binary version, which is, of course, our aim here.

We test neither the original ED method nor the basic version of the MECA because they do not generate blue noise as well as their randomly perturbed versions.

### 3 Numerical experiment

In the first stage of our experiment, six binary filters are generated on a rectangular grid. The binary filters are supposed to substitute a super-resolving parabolic continuous-tone filter whose amplitude transmittance is

$$t(u,v) = \text{circ} \left( \frac{\sqrt{u^2 + v^2}}{R} \right) \frac{u^2 + v^2}{R^2}, \quad (8)$$

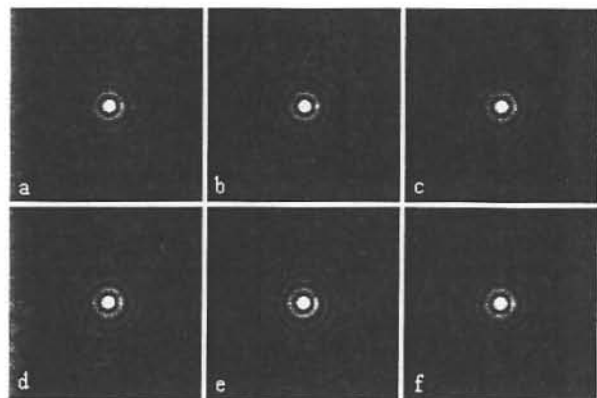


FIGURE 9 — Squared moduli of the AIRs of binary filters. In the upper-left quadrants the  $|AIR|^2$  of a continuous-tone filter are shown.

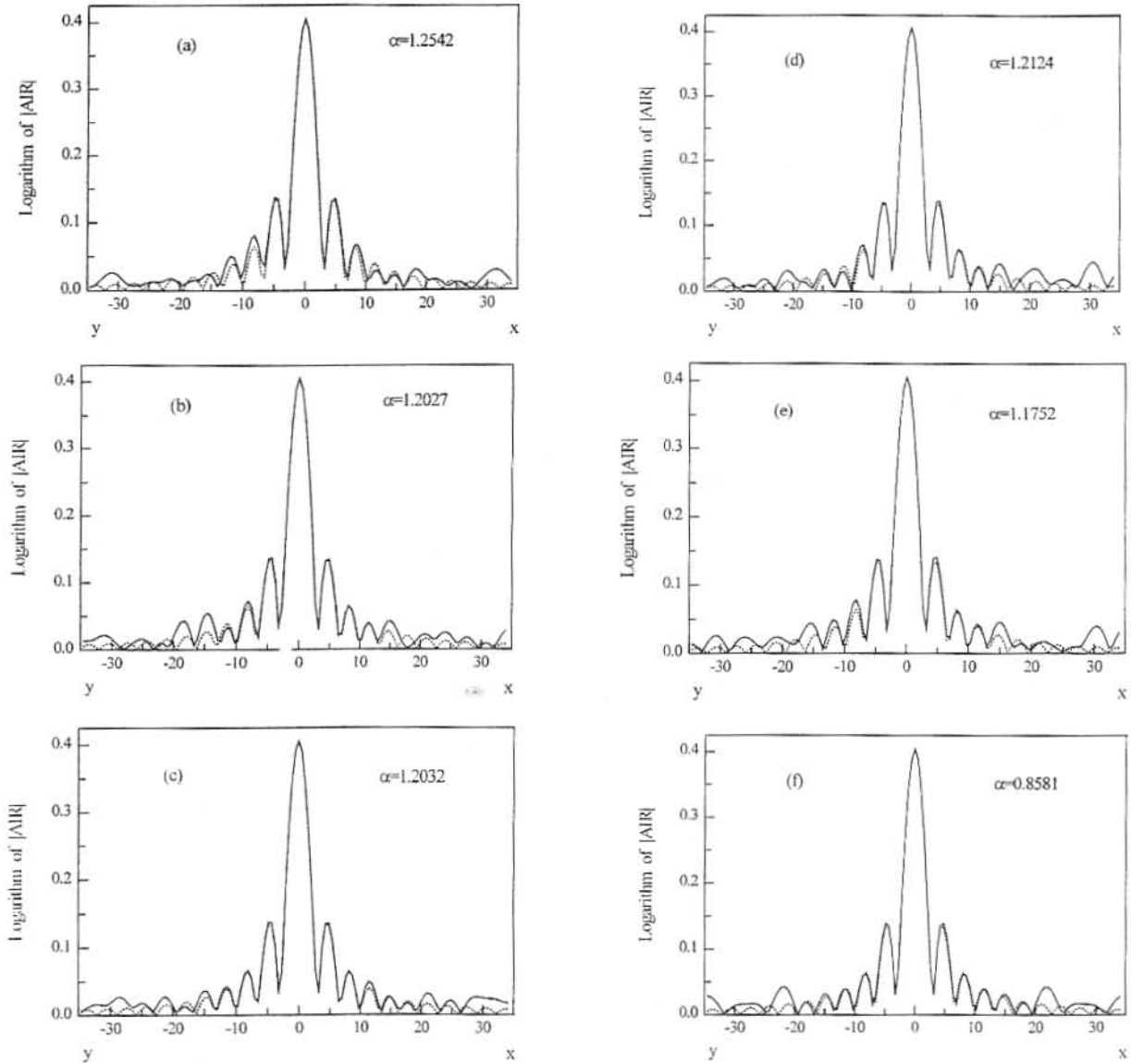


FIGURE 10 — Cross sections of intensity distributions in the image of a point source obtained with the binary pupil filters shown in Fig. 8 (logarithmic scale). We present the intensity distribution along semi-axes  $0x$  and  $0y$  to reveal possible deviations from radial symmetry. The dotted line corresponds to  $F(x, y)$  and solid line to  $\alpha G(x, y)$ .

where  $(u, v)$  are the spatial coordinates in the filter plane and  $R$  is the radius of the filter. The coherent transfer function of the  $4f$  imaging system with such a filter in the Fourier plane (Fig. 7) is equal to

$$P(\mu, \nu) = t(\mu\lambda f, \nu\lambda f) = \text{circ} \left( \frac{\sqrt{\mu^2 + \nu^2}}{\rho_c} \right) \frac{\mu^2 + \nu^2}{\rho_c^2}, \quad (9)$$

where  $(\mu, \nu)$  are the spatial-frequency coordinates in the Fourier plane and  $\lambda$  is the wavelength of the coherent illu-

minating beam. At the cutoff frequency of the system,  $\rho_c = R/\lambda f$ , the parabolic transfer function  $P(\mu, \nu) = 1$ . The super-resolving binary filters obtained with (a)–(f) algorithms are shown in Fig. 8. It is seen that the only filter that preserves the symmetry of the clear pupil (built with squared cells, as shown in Fig. 5) is that obtained with the IFTA, which is the unique parallel-processed deterministic algorithm tested here.

In the second stage, we calculate the intensity distributions in the images of a point source obtained in the  $4f$  imaging system, placing subsequent binary filters in the

Fourier plane. That is, we calculate the squared modulus of the AIR of each binary filter. The intensity distributions are shown in Fig. 9, where they are qualitatively compared with that obtained for the graytone filter.

Quantitative comparison is shown in Figs. 10(a)–10(f), where the moduli of corresponding AIRs are drawn in logarithmic scale.

In order to evaluate the resemblance of the AIRs of binary filters to the AIR of their graytone counterpart, we use the signal-to-noise ratio (SNR) as proposed by Weissbach and Wýrowski<sup>9</sup>:

$$\text{SNR} = \frac{\iint_A [F(x,y)]^2 dx dy}{\iint_A [F(x,y) - \alpha G(x,y)]^2 dx dy} \quad (10)$$

where coefficient

$$\alpha = \frac{\iint_A F(x,y)G(x,y) dx dy}{\iint_A [G(x,y)]^2 dx dy} \quad (11)$$

maximizes the SNR. In our calculations,  $F(x,y)$  is the squared modulus of the AIR of the continuous-tone filter and  $G(x,y)$  is  $|\text{AIR}|^2$  of the binary one. The squared area  $A$  is centered at the optical axis and its side is equal to the diameter of the second zero ring of  $T(x,y)$ . The AIRs of binary filters are calculated with the FFT, where the diameter of the filter and the size of matrix of pixels are the same as those used in the iterative Fourier-transform algorithm. We use the SNR defined in Eqs. (10) and (11) as a merit function which orders all algorithms according to the degree of resemblance between the AIR of corresponding binary filters and that of the continuous one. In Fig. 10 it is seen that over the area  $A$ , the distributions  $\alpha G(x,y)$  coincide almost perfectly with  $F(x,y)$ . Therefore,  $\alpha^{-1}$  can be considered a ratio between the light efficiency of the binary pupil filter and that of the underlying

graytone filter. By the light efficiency we mean here the fraction of incident energy which falls into the signal window  $A$ .

The values of the SNR and  $\alpha^{-1}$  are presented in Table 2. In the case of algorithms that use random-number generators [(a)–(e)], we generated ensembles consisting of 100 sample filters. In Table 2, we show the SNR of the best sample selected from the ensemble, which is the very sample shown in Fig. 8. In Table 2, we also present the average signal-to-noise ratio,  $\overline{\text{SNR}}$ , and the standard deviation of SNR,  $\sigma_{\text{SNR}}$ , that characterize the entire ensemble.

Finally, the performance of the binary filters is examined in terms of the two-point Sparrow resolution criterion for coherent illumination. To this end we performed a numerical experiment in which two coherent point sources are located in the object plane of the imaging system shown in Fig. 7. The points are spaced  $2b$  apart. Then for each filter, we calculate the minimum value of  $2b$  allowed by the Sparrow criterion (see Table 2). In Table 2, the deviations  $\Delta b$  of the value  $2b$  from  $2b_r$ , where  $2b_r = 4.295$  is the resolution limit calculated for the continuous parabolic filter, are also presented.

## 4 Conclusions

From the wide scope of existing digital-half-toning techniques, we have selected a subset of procedures (which belong to four different categories), which are well adapted to the purpose of binarizing continuous-tone pupil filters. Next, in order to evaluate the resemblance of the AIRs of binary filters to the AIR of their continuous-tone counterpart, we have defined a merit function, the SNR. Then, after a numerical simulation, we have obtained the following results.

The resemblance between the spectrum of a continuous super-resolving parabolic pupil filter and that of its binary version strongly depends on the binarization algorithm. For six filters generated with six different algorithms analyzed here, the SNR, which is the quantitative measure of this resemblance, varies from 949 to 5775. The resemblance achieved for pupil filters generated with randomly perturbed ED algorithms processed on a serpentine raster is higher than that for dithering with white noise and the IFTA. The best realization (chosen from the ensemble of 100 samples) was generated with only one randomly positioned weight [algorithm (b)]. This algorithm is characterized by the highest standard deviation of SNR. Therefore, the probability that one will generate the binary filter whose SNR considerably exceeds the average SNR, which for this algorithm is quite good, is relatively high. The best two, from the point of view of the SNR [algorithms (b) and (d)], in fact belong to the same class of ED with random perturbations. This is because the error filter with one randomly positioned weight is equivalent to a two-weight filter whose weights are 100% perturbed. Namely, we have one pair of weights (1/2, 1/2) which is perturbed as follows:

TABLE 2 — The SNR, resolution limit, and relative light efficiency for (a)–(f) algorithms.

Algorithm	SNR	$\overline{\text{SNR}}$	$\sigma_{\text{SNR}}$	Two-point resolution $2b$ (deviation $\Delta b$ )	Relative light efficiency ( $\alpha^{-1}$ )
(b)	5775	1756	573	4.294 [-0.001]	0.831
(d)	4370	1931	570	4.323 [0.028]	0.825
(c)	3429	1708	508	4.323 [0.028]	0.831
(e)	2287	528	293	4.332 [0.037]	0.851
(f)	1420	—	—	4.364 [0.069]	1.165
(a)	949	246	150	4.320 [0.025]	0.797

$$\left(\frac{1}{2}, \frac{1}{2}\right) \rightarrow \left(\frac{1}{2} + b\chi, \frac{1}{2} - b\chi\right); \quad (12)$$

in this case,  $\chi$  takes on with equal probability the values 0.5 and -0.5, whereas  $b = 1$ .

All the filters we have generated demonstrate super-resolving properties (for the clear pupil,  $2b = 4.600$ ). For the algorithm (b), the value  $2b = 4.294$  coincides almost perfectly with the corresponding theoretical value  $2b_t = 4.295$ . From Table 2, the correlation between the SNR and the deviation  $\Delta b$  is rather weak, at least within the range of the SNR we deal with. Perhaps the explanation of this is as follows. The binary filters are not rotationally symmetric, so the two-point resolution that can be obtained depends on the angular orientation of the filter with respect to the direction determined by the straight line which passes through both point sources. On the other hand, the SNR involves integration; hence, it averages angular effects. When the SNR is high, there are no essential differences between favorable and unfavorable (from the point of view of resolution) angular orientation of the filter.

From the analysis of data in the outermost right-hand column of Table 2, it is shown that binarization may lead to improvement of light efficiency. It is seen that the light efficiency of the binary pupil generated by the IFTA is higher than that of the graytone filter by about 17%. However, our opinion is that the light-efficiency ratio  $\alpha^{-1}$  can be used as a merit function only when comparing binarization methods with similar values of SNR.

In order to find the procedure which would maximize our merit function, we tested five already known and one new procedure proposed by us [algorithm (d)]. We showed that the new procedure, being a modification of (c), yields a higher value of SNR than the original version. Moreover, the algorithm (d) is characterized by the highest SNR. Nevertheless, the highest values of SNR, which are six times higher than that for the technique considered best until now (a), are achieved for the error diffusion with one randomly positioned weight. We believe that further improvements of binarization techniques and in particular of the IFTA and MECA are possible. From Ref. 17, if we use the IFTA, the convergence of partially binarized patterns  $U^{(p)}t_j(u,v)$ , and the form of binary limit distribution  $U^{(0.5)}t_{j_{\max}}(u,v)$  depend on the topology of a given problem and the initial distribution  $t_0(u,v)$ . Therefore, some manipulations are still possible. Regarding the MECA, a systematic study of this procedure could lead to the further improvement, but a general analytical approach is needed. Although MECA can be considered a type of ED procedure, the Weissbach and Wyrowski approach can't be applied here because it is valid only for algorithms processed sequentially, whereas the MECA is processed in parallel.

## Acknowledgment

Marek Kowalczyk carried out his research as part of the European Economic Community action Go West financed by the Commission of the European Communities under the contract ERB-CIPA-CT-92-0135.

This work was partially supported by the Dirección General de Investigación Científica y Técnica (Grant PB93-03445-CO2-01), Ministerio de Educación y Ciencia, Spain.

## References

- 1 P Jaquinot and B Roizen-Dossier, "Apodisation," in: *Progress in Optics*, Vol. III, E. Wolf, ed (North Holland, Amsterdam, 1964).
- 2 Z S Hegedus, "Annular pupil arrays. Application to confocal scanning," *Opt Acta* **32**, 815-826 (1985), and references therein.
- 3 T W Barnard, "Binary imagery and its applications to beam shaping," *Appl Opt* **10**, 2274-2278 (1971).
- 4 Z S Hegedus, "Pupil filters in confocal imaging," in: *Confocal Microscopy*, T Wilson, ed (Academic, London, 1990), pp. 171-183.
- 5 R Ulichney, *Digital Halftoning* (MIT Press, Cambridge, 1987).
- 6 D Kermisch and P G Roetling, "Fourier spectrum of halftone images," *J Opt Soc Am* **65**, 716-723 (1975).
- 7 M Broja and O Bryngdahl, "Quantization noise in electronic halftoning," *J Opt Soc Am*, A **4**, 554-560 (1993).
- 8 Y Pinhasi and D Peri, "A generalized analysis of binary halftone representation of images," *Opt Commun* **101**, 277-285 (1993).
- 9 S Weissbach and F Wyrowski, "Error diffusion procedure: theory and application in optical signal processing," *Appl Opt* **31**, 2518-2534 (1992).
- 10 T Mitsa and J Parker, "Digital halftoning technique and blue-noise mask," *J Opt Soc Am A* **9**, 1920-1929 (1992).
- 11 M Kowalczyk, P Andrés, and M Martínez-Corral, "Apodization of imaging systems by means of a random spatially nonstationary absorbing screen," *J Opt Soc Am A* **9**, 1930-1936 (1992).
- 12 C Billotet-Hoffmann and O Bryngdahl, "On the error-diffusion technique for electronic halftoning," *Proc SID* **24/3**, 253-258 (1983).
- 13 E Menzel and K Pietzsch, "Space variant optical transfer with Fourier filter in extrapupilar position," *Optik* **46**, 451-461 (1976).
- 14 R Barakat, "Application of apodization to increase two-point resolution by the Sparrow criterion. I. Coherent illumination," *J Opt Soc Am* **52**, 276-283 (1962).
- 15 E Peli, "Multiresolution error-convergence halftone algorithm," *J Opt Soc Am A* **8**, 625-636 (1991).
- 16 M Broja, F Wyrowski, and O Bryngdahl, "Digital halftoning by iterative procedure," *Opt Commun* **69**, 205-210 (1989).
- 17 T Peter, F Wyrowski, and O Bryngdahl, "Importance of initial distribution for iterative calculation of quantized diffractive elements," *J Mod Opt* **40**, 591-600 (1993).



Marek Kowalczyk received his M.Sc. degree in Physics from Nicolaus Copernicus University in Torun, Poland. In 1980 he joined the Image Processing Group at the University of Warsaw. He received his Ph.D. in Physics in 1985 from the University of Warsaw. He studied holography, holographic memory systems, image processing, and spectral and imaging properties of phase objects in coherent optical systems. Dr. Kowalczyk's current interests include statistics of laser speckle phenomena, speckle velocimetry, and application of statistical methods in digital halftoning.



**Tomasz Cichocki** received his M.Sc. degree in Physics from the University of Warsaw, Warsaw, Poland in 1992. At present he is a Ph.D. student at the Image Processing Group, Institute of Geophysics, the University of Warsaw, Warsaw, Poland. His interests include digital-half-toning methods and spatial and temporal properties of optical-digital processors.



**Manuel Martínez-Corral** received his M.S. and Ph.D. degrees in Physics from the University of Valencia, Burjassot, Spain, in 1988 and 1993, respectively. He joined the University of Valencia in 1989, and has since worked in the area of optical information processing. Currently, he holds the position of assistant professor.